



**HAL**  
open science

## Activation volume and energy of bulk metallic glasses determined by nanoindentation

Lisa Krämer, Verena Maier-Kiener, Yannick Champion, Baran Sarac,  
Reinhard Pippan

► **To cite this version:**

Lisa Krämer, Verena Maier-Kiener, Yannick Champion, Baran Sarac, Reinhard Pippan. Activation volume and energy of bulk metallic glasses determined by nanoindentation. *Materials & Design*, 2018, 155, pp.116-124. 10.1016/j.matdes.2018.05.051 . hal-01807726

**HAL Id: hal-01807726**

**<https://hal.science/hal-01807726>**

Submitted on 23 Feb 2023

**HAL** is a multi-disciplinary open access archive for the deposit and dissemination of scientific research documents, whether they are published or not. The documents may come from teaching and research institutions in France or abroad, or from public or private research centers.

L'archive ouverte pluridisciplinaire **HAL**, est destinée au dépôt et à la diffusion de documents scientifiques de niveau recherche, publiés ou non, émanant des établissements d'enseignement et de recherche français ou étrangers, des laboratoires publics ou privés.



Distributed under a Creative Commons Attribution - NonCommercial 4.0 International License

# Activation volume and energy of bulk metallic glasses determined by nanoindentation

Lisa Krämer <sup>a,\*</sup>, Verena Maier-Kiener <sup>b</sup>, Yannick Champion <sup>c</sup>, Baran Sarac <sup>a</sup>, Reinhard Pippan <sup>a</sup>

<sup>a</sup> Erich Schmid Institute of Materials Science, Austrian Academy of Sciences, Leoben, Austria

<sup>b</sup> Department Physical Metallurgy and Materials Testing, Montanuniversität Leoben, Austria

<sup>c</sup> Univ. Grenoble Alpes, CNRS, Grenoble INP, SIMaP, F-38000 Grenoble, France

Nanoindentation strain-rate jump testing was used to determine activation volumes and energies of various metallic glasses and composites. Three different single phase metallic glasses and three composites (two with amorphous/crystalline Cu and one with an amorphous/amorphous structure) were investigated. The state of the materials was additionally changed by varying the testing temperature between room temperature and 430 °C, by performing high pressure torsion and by thermal cycling. The results show that testing temperature is the main parameter controlling activation volume and energy, whereas material modifications by high pressure torsion and thermal cycling do not significantly affect them.

## 1. Introduction

Bulk metallic glasses (BMG) have no long-range order due to their amorphous structure, but it has been shown numerously that their short-range order is of great importance. By changing the short-range

order and therefore the state of the metallic glass, intrinsic properties such as hardness or toughness can be changed [1,2]. The state of BMGs can be changed by varying the composition, casting conditions or additional annealing and rejuvenating treatments [3–6]. Rejuvenation of BMGs can be achieved by thermal cycling or deformation [3,7]. One of the most effective techniques for achieving the latter is high-pressure torsion (HPT). A disc-like specimen is placed between two anvils which are rotated against each other under high pressure of more

\* Corresponding author.

E-mail address: lisa.kraemer@oeaw.ac.at (L. Krämer).

than three times the yield stress of the material, for details see [8,9]. Due to its nearly hydrostatic pressure, enormous equivalent shear strains higher than 20,000 can be applied. Even materials which are brittle and fail catastrophically under standard deformation conditions can be deformed with HPT. This makes the technique interesting for optimizing BMGs and producing bulk metallic glass composites (BMGCs) [10–12]. To quantify the influence of changing the short-range order and free volume, different techniques such as transmission X-ray diffraction during cyclic heating [13] or creep testing [14], positron annihilation spectroscopy [15] and DSC [16] have been used. Nanoindentation is commonly used to determine activation volume and energy of crystalline materials by using different strain rates for testing. Maier et al. suggested using different strain rates during indentation and therefore, the testing time could be shortened significantly, but this technique also allows probing of selected regions with different strain rates, which can be important for heterogeneous materials [17]. Therefore, strain rate sensitivity and consequently the activation volume can be determined by means of only a single indent [18]. During nanoindentation of BMGs, a serrated flow behavior often occurs, and Wright et al. concluded that each serration was the onset of a shear band [19]. These serrations or pop-ins depend on strain rate and temperature, but they are similar in frequency and size for different BMGs if the testing was conducted at the same homologous temperature ( $T/T_g$ , where  $T$  is the testing and  $T_g$  is the glass transition temperature) [20–23]. Annealing of BMGs decreases the free volume and increases Young's modulus and hardness, but no significant effect on the serration behavior during nanoindentation is detectable [24]. Not only the strain rate, but also the tip geometry [25] and residual stresses [26,27] influence the number and size of the serrations. Different methods have attempted to evaluate the serration behavior and try to link it to the deformation behavior of the BMGs, such as the examination of the first pop-in for different strain rates using a cooperative shear model [28], the evaluation of the first pop-in depending on a critical strain by using a spherical indenter [29] or the use of a mean field model to link the slip avalanches to annealing temperatures [30]. In literature, activation volumes for BMGs were also obtained by evaluating the depth variation during a constant load experiment by nanoindentation [31], nanoindenter cantilever bending and mandrel bend relaxation techniques [32], pseudo-creep and compression testing with different strain rates at elevated temperatures [33], and three point bending tests at different temperatures [34].

The aim of this study was to elucidate whether small-scaled strain rate jump tests by nanoindentation can be used reliably to calculate activation energy and volume for plastic deformation in BMGs. Considering the amorphous structure, a different approach than for crystalline materials is proposed. The influence of composition was investigated by means of three different bulk metallic glasses, as well as the influence of a second phase by testing three different BMGCs (two with crystalline Cu and one with another MG as the second phase). Two specimens were additionally subjected to HPT and two to thermal cycling. The main questions that will be addressed are: How do the activation energy and volume differ for different compositions and fabrication methods? How does a second phase influence these two properties? How do the properties vary with the testing temperature? And have HPT-deformation and thermal cycling an influence on activation volume and energy?

## 2. Experimental

Three Zr-based and one Ni-based MGs were investigated. ZrBe-MG ( $Zr_{35}Ti_{30}Cu_{7.5}Be_{27.5}$ ) was rod cast with 10 mm diameter [35–37]. Zr-MG ( $Zr_{57}Cu_{20}Al_{10}Ni_8Ti_5$ ) and Ni-MG ( $Ni_{53}Nb_{20}Ti_{10}Zr_8Co_6Cu_3$ ) samples were produced from amorphous powders (high pressure gas atomization [38]) with subsequent consolidation and deformation by HPT to achieve bulk samples. By this method, composites containing the Zr-MG and Ni-MG or Zr-MG and crystalline Cu can also be fabricated. This process and the evolution of their microstructures are described

in detail in previous papers [10–12]. For this study, samples with between 30 and 50 turns of deformation by HPT were used. The single-phased BMGs generated from powders require a minimal strain to ensure fully consolidated samples [12]. For the amorphous/crystalline and amorphous/amorphous composites, the applied strain is even more important for the microstructural evolution. The shear strain and pressure cause consolidation and a lamellar structure of the different phases, which refines as the applied strain is increased. This increase in strain can be realized by either increasing the number of turns in the HPT-process or by investigated the samples at a larger radius. At large strains, mixing of the two phases occurs, which leads at very high applied shear strains to saturation resulting in a single-phased amorphous material for Zr-MG 20 wt% Cu and Ni-MG 30 wt% Zr-MG. The saturation microstructure of Zr-MG 80 wt% Cu contains nanocrystalline supersaturated solid solution Cu in which elongated Zr-MG bands are embedded. Since we are interested in the effect of composites on the activation volume and energy for this study, the testing area was chosen where the phase spacing was smaller than the imprints of the nanoindentation, but where the two phases are not fully mixed. Furthermore, it was tried for each sample to minimize the variation of the radius at which the indents were performed to probe comparable microstructures. In Fig. 1, representative scanning electron microscopy (SEM) micrographs of the microstructure of the three composites (Zr-MG 20 wt% Cu, Zr-MG 80 wt% Cu, and Ni-MG 30 wt% Zr-MG) are shown. Due to the oxidation of the surface, the fine microstructure is not clearly visible after high temperature testing.

One ZrBe-MG specimen was deformed by HPT for 20 turns to investigate the influence of predeformation.

One Zr-MG and one Ni-MG sample were thermally cycled by cooling with liquid nitrogen for 1 min and then heating with a hot-air gun to room temperature for 1 min.

Differential Scanning Calorimetry (DSC) was conducted for 15 mg pieces of Zr-MG and ZrBe-MG using a heating and cooling rate of  $10 \text{ K s}^{-1}$  (Mettler Toledo DSC3+). The results show a glass transition temperature of  $405 \text{ }^\circ\text{C}$  and  $290 \text{ }^\circ\text{C}$ , respectively. For Ni-MG literature indicates a  $T_g$  of approximately  $571 \text{ }^\circ\text{C}$ , which is significantly higher than the maximum nanoindentation testing temperature [39].

For micromechanical investigations, the surface was ground and polished. The nanoindentation testing was limited to regions of the same applied strain for HPT-deformed samples, thus at the same radius of the deformed disks. The as-cast sample was probed in the central region to avoid influences from the cast surface. For all depth sensing hardness testing experiments, a platform nanoindenter G200 (Keysight Tec, USA) equipped with CSM (continuous stiffness measurement) Young's modulus as well as a Laser Heating stage (Surface Tec, Hückelhoven, Germany) was used. Latter one allows the independent heating of the indentation tip and the sample, which ensures a fine adjustment of both temperatures to precisely adjust the exact contact temperature. Thus, possible thermal drift can be further minimized even at elevated temperatures [40]. The testing temperatures were varied between room temperature and  $430 \text{ }^\circ\text{C}$  and the intervals were chosen according to the transition in mechanical properties respectively for each specimen. Moreover, at elevated temperatures tip and sample were independently but continuously jetted with forming gas in order to minimize any oxidation reactions on the surface. For room temperature tests, the system was equipped with a diamond Berkovich tip (Synton-MPD, Switzerland), while for elevated temperature testing a sapphire Berkovich tip (Synton-MPD, Switzerland/Surface Tec, Hückelhoven) was used in order to minimize chemical reactions between tip and sample at higher temperatures [41]. All indentations were generally conducted under strain rate controlled conditions and with abrupt, repetitive changes in the applied strain rate ( $\dot{\epsilon} = \frac{\dot{h}}{h} = \frac{\dot{P}}{2P}$ ) [42] to a maximal indentation depth of 2500 nm. For this study the strain rate was changed after every 500 nm of the indentation

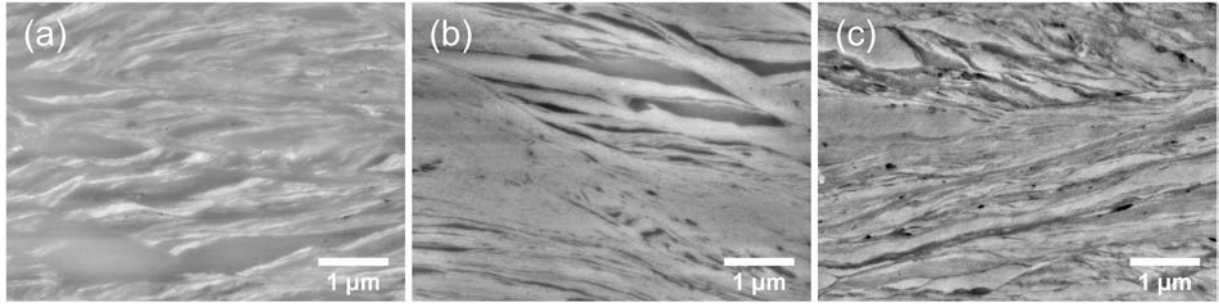


**Fig. 1.** SEM micrographs of representative microstructure of the three tested composites. (a) Zr-MG 20 wt% Cu, (b) Zr-MG 80 wt% Cu and (c) Ni-MG 30 wt% Zr-MG. HPT-deformation causes a gradual refinement along the radius and therefore, a variation of the tested microstructure is not preventable. The side length of a Berkovich indents is approximately 15  $\mu\text{m}$ .

depth with different profiles for room temperature [17]: 0.025–0.0025 – 0.025–0.0005 – 0.025  $\text{s}^{-1}$  and for elevated temperatures [43]: 0.025–0.005–0.025–0.0025–0.025  $\text{s}^{-1}$ . Hardness and Young's modulus were measured continuously over indentation depth with a CSM unit, where a sinusoidal load signal is superimposed to the load displacement data and the data were corrected according to Pharr et al. [44]. All data were evaluated according to the method of Oliver and Pharr [45] using a Poisson ratio of 0.37 to calculate the Young's modulus and the averaged data were calculated from the third strain rate regime between indentation depths from 1050 to 1450 nm for a strain rate of 0.025  $\text{s}^{-1}$ .

One minor problem occurring during testing was a slight break out at the very end of the high temperature sapphire Berkovich indenter just before testing the ZrBe-MG. Thereby, the tip calibration became inaccurate for the testing series at elevated temperature of this material. This influence is clearly seen for the Young's modulus as a function of the indentation depth especially at smaller indentation depth and lower temperatures. Nevertheless, the data from larger indentation depths were used qualitatively, as the overall trend of the measured and calculated properties is similar to the other tested materials.

### 3. Results

#### 3.1. Evaluation of the strain rate jump tests

Nanoindentation was conducted on above described different BMGs and BMGCs samples. Changes in deformation mechanism were investigated by changing the testing temperatures and the history of the samples using HPT or thermal cycling. To estimate activation volume and activation energy, an equation proposed by Spaepen [46] was used. This equation links the plastic flow rate with a net jump frequency of flow defects under the influence of stress:

$$\dot{\gamma} = n\gamma_0 v_0 k_a \sinh \frac{\tau v_0 \gamma_0}{kT} e^{-\frac{\Delta G}{kT}} \quad (1)$$

where  $n$  is the concentration of flow defects,  $\gamma_0$  the shear strain produced by rearranging of a flow defect,  $v_0$  is the volume of a flow defect,  $k_a$  the jump frequency,  $\tau$  the shear stress,  $k$  the Boltzmann constant and  $\Delta G$  the activation energy. The advantage of this equation is its generality, as the flow defects can be single atoms, dislocations in crystalline metals or shear transformation zones in metallic glasses. The flow defects vibrate due to thermal energy and at higher temperature  $\Delta G$  can be overcome (exponential part of Eq. (1)), which leads to local shearing. At lower temperature, an additional energy for moving flow defects is necessary. Mechanical stress on the flow defects are represented as a hyperbolic energy term. This hyperbolic part leads to a favored jump direction for the flow defects and therefore to a higher numbers of jumps in one direction than in another. Langer [47] pointed out that this equation neglects several aspects such as anisotropy and heterogeneity of the material, but we assume it is valid for an estimation of dominating deformation processes in metallic glasses.

By applying different strain rates, it is possible to simplify Eq. 1 to

$$\frac{\dot{\gamma}'}{\dot{\gamma}} = \frac{n'\gamma_0' \sinh \frac{\tau' v_0 \gamma_0'}{kT}}{n\gamma_0 \sinh \frac{\tau v_0 \gamma_0}{kT}} \quad (2)$$

where the variables with and without prime are measured for two different strain rates. Strain rate jump tests were conducted at different temperatures. In Fig. 2 measurements of Zr-MG at two different temperatures are shown. Hardness ( $H$ ), Young's modulus ( $E$ ), and load are plotted as a function of indentation depth. Blue, dashed lines mark the different strain rates and the respective values are at the top of the figure. In the upper two subplots, hardness and Young's modulus are plotted. The Young's modulus remains constant over the whole indentation depth and the change in the strain rate causes different scattering of the data. At 400 °C, the Young's modulus is slightly decreased compared to 100 °C, but the effect of temperature on hardness is more distinct. Increasing the temperature from 100 °C to 400 °C, leads to a strong decrease in hardness. Additionally, the hardness becomes dependent on the strain rate. This strain rate sensitivity can be deduced from the load - indentation depth curves, where a change in the strain rate causes a change in the slope of the curve. At lower temperature, the BMG shows serrations in the load curve and corresponding boosts and drops in hardness. At 400 °C the curves for the load and the hardness are significantly smoother.

The size and number of the serrations decrease with increasing temperature. For further evaluation, the shear strain of one flow unit is calculated from  $\gamma_0 = \frac{d_s}{h}$ , where the definition of  $d_s$  and  $h$  are given in Fig. 2. Yang et al. showed that the serration size depends linearly on the indentation depth [48]. Therefore,  $d_s$  was not measured at small indentation depths, as the resolution of the instruments is probably not high enough for distinctive shear bands. Also the distance between two serrations (in 2 the distance between two neighboring red dots) depends directly on the indentation depth. In c and f, the distance of two neighboring data points divided by the indentation depth is plotted as a function of the indentation depth. Most of the data points have similar distances to their neighboring ones, but obviously each serration increases the distance. Therefore, data points showing extrema in the neighboring distance are used to determine  $d_s$ . Additionally, the linear dependence of the serration size on the indentation depth is used to calculate the concentration of serrations as the distribution of serrations follows a geometric progression with

$$h_n = h_0(1 + \bar{q})^n \quad (3)$$

$$\bar{q} = \frac{1}{m} \sum_{i=1}^m \frac{h_i - h_{i-1}}{h_i} \quad (4)$$

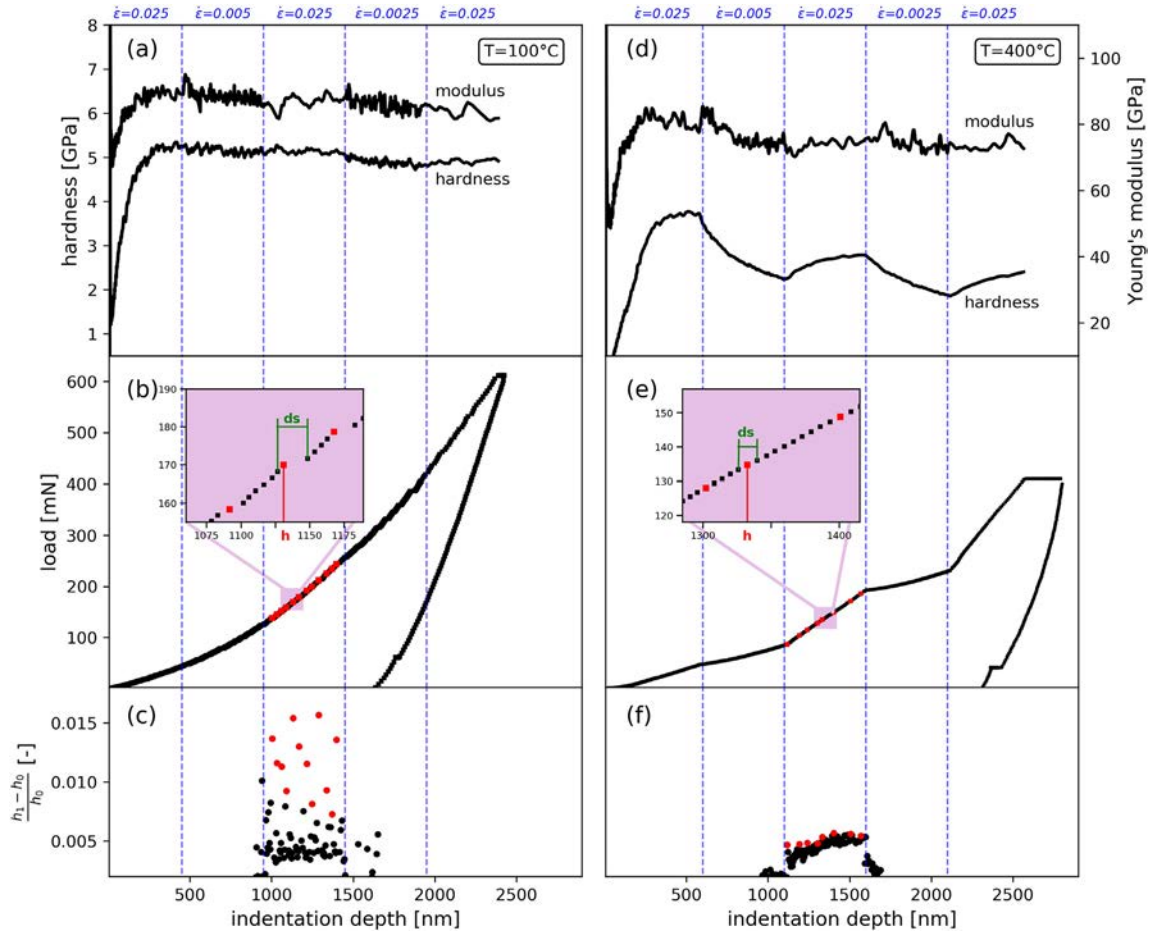


**Fig. 2.** (a and d) Hardness, Young's modulus and (b and e) load as a function of indentation depth for two representative strain rate jump test for Zr-MG at two different temperatures (100 °C on the left and 400 °C on the right). One indent was conducted with three different strain rates (0.025, 0.005, and 0.0025 s<sup>-1</sup>) over the course of 5 segments, which illustrate the temperature dependent hardness and serration behavior. The determination of serration size and serration position can be found in (c and f) and the two insets.

$\bar{q}$  can be estimated from Fig. 2, and to obtain a concentration,  $n$  for  $h = \sqrt[3]{3/24.5} \text{ m}$  is calculated.  $h$  is the height of a pyramid formed as Berkovich indenter with a volume of 1 m<sup>3</sup>.

For solving Eq. 2, only the shear stress is missing. Tabor already estimated that the hardness correlates to the strength by a factor of 3 [49]. To take into account the change from a more elastic to a more plastic behavior, a method recently refined by Leitner et al. was used [50]. The fraction of plastic deformation can be estimated from the nanoindentation test carried out in CSM mode and is used to calculate the constraint factor,  $c^*$ , which varies between 1 and 2.91. The constraint factor depends on the testing temperature and was used to estimate  $\tau$  from the measured hardness for all strain rates.

$$\tau = \frac{H}{c^* \sqrt{3}} \quad (5)$$

To verify this approach, the activation volume for a Cu sample was calculated via the method proposed here and via an accepted method using the strain rate sensitivity [51]. The calculated activations volumes are  $294 \pm 21 \text{ b}^3$  and  $324 \pm 50 \text{ b}^3$  ( $b = 0.2555 \text{ nm}$ , burgers vector for Cu), respectively. For calculating the activation energy only the jump frequency of the atoms is missing. This can be estimated by approximating each atom as a harmonic oscillator with an energy of  $E = 3kT$  and taking the maximal displacement  $\Delta x$  at each temperature via the thermal expansion of the materials ( $\Delta x = \alpha r \Delta T$ , with  $r$  as the atomic radius).

The frequency  $k_a$  is then calculated with the atomic mass,  $m$ , by

$$k_a = \sqrt{\frac{6k}{mT}} * \frac{1}{2\pi\alpha r} \quad (6)$$

The calculated frequencies are just an estimation, because only the main elements of the glasses were taken into the account for atomic mass and radius, and additionally, the thermal expansion changes drastically as soon as  $T_g$  is approached [52–54]. However, the calculated values are in the range of  $10^{13} \text{ s}^{-1}$  as expected and show a falling tendency with temperature.

### 3.2. Influences of the temperature

Three to four indentations were performed at each testing temperature and mean values were used for calculation. For some materials more than one sample was tested to validate the repeatability of the data evaluation and once more, only their mean value was used furthermore. In Fig. 3, the concentration of the flow units (a-c) and their shear strain (d-f) are plotted for all three strain rates as a function of temperature. For smaller strain rates, the concentration of flow units is higher, but the local shearing is less ( $d_s/h$ ). At temperatures approaching the glass transition temperature, the concentration of flow units for small strain rates decreases and approaches the value of the highest strain rate. On the contrary,  $d_s/h$  decreases for higher strain rates as the temperature comes into the range of glass transition.

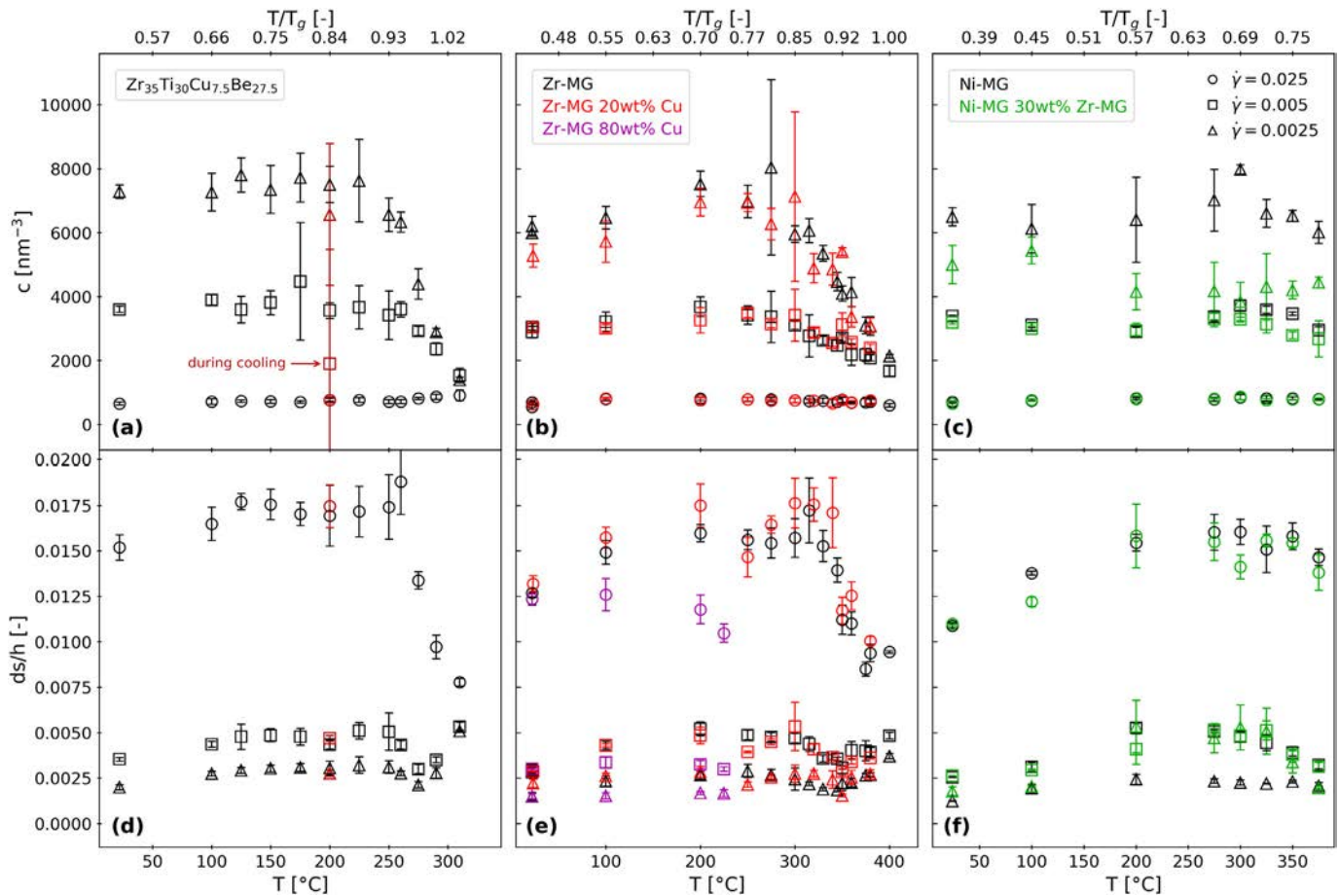


**Fig. 3.** Concentration and normalized size of serrations as a function of the indentation temperature. The concentration and shear strain of the flow units depends on the strain rate. Higher strain rates lead to less activated flow units, and higher shear strains per unit. For lower strain rates the situation is reversed.

In Fig. 4d-f, hardness and Young's modulus are plotted versus the testing temperature. The Young's modulus of Ni-MG and the composite Ni-MG 30 wt% Zr-MG (c) stay nearly constant even at high temperatures. Moreover, only a slight softening is observed. The softening of Zr-MG (b) and ZrBe-MG (a) is more pronounced especially for the latter, because the testing temperature exceeds their  $T_g$ . The Young's modulus decreases slightly with increasing testing temperature for both Zr-based MGs and again it is more pronounced for ZrBe-MG. For the composite Zr-MG 20 wt% Cu, values and behavior of hardness and Young's modulus are nearly identical to the ones of the single phase Zr-MG. Zr-MG 80 wt% Cu shows the drop in hardness and Young's modulus already at 200 °C.

Activation volume and activation energy are plotted in Fig. 4a-c. The activation volume for all tested materials stays constant as a function of the temperature until  $T_g$  is approached. Then the activation volume increases drastically and for ZrBe-MG (a) an increase of 20 times for a temperature increase of 20 °C is observed. For Zr-MG and Zr-MG 20 wt% Cu (b), the curve looks similar as ZrBe-MG, but the change is more moderate. Zr-MG 80 wt% Cu already shows a decrease in hardness at temperatures above 200 °C, but as the samples were heavily oxidized, no measurements at higher temperatures could be conducted. Ni-MG and Ni-MG 30 wt% Zr-MG (c) show no increase in the activation volume and their activation energy increases steadily with temperature. It should be noticed that Ni-MG has a higher  $T_g = 573$  °C [55] than the highest possible testing temperature. Their activation energy increases steadily with temperature. ZrBe-MG shows lower  $\Delta G$  at  $T_g$  than Zr-MG, and  $\Delta G$  of Ni-MG is already higher even though the homologous temperature is lower. The activation energy of the composites matches the respective single phased BMGs.

### 3.3. The influence of the applied strain during HPT

ZrBe-MG was deformed via HPT for 15 rotations. By testing at different radii, the material with varying applied strains was probed. In Table 1, Young's modulus, hardness, activation volume, and activation energy of ZrBe-MG at room temperature for three different applied strains are listed. Young's modulus and hardness are slightly increased, but the activation volume and energy show no clear trend. Therefore, it must be concluded that no significant changes are detectable.

### 3.4. Influence of thermal cycling

In Fig. 5, hardness, Young's modulus and activation volume of thermally cycled specimens are shown. A variation depending on the number of cycles can be seen, but the changes are small and no clear trend is evident. Ni-MG shows a minimum in hardness at 2 cycles, no change in the Young's modulus and a more random behavior for the activation volume. Zr-MG shows a minimum in hardness at 10 cycles, a minimum in Young's modulus for 5 cycles and two plateaus with the transition between 5 and 10 cycles for the activation volume.

## 4. Discussion

Three different BMGs with different glass transition temperatures (ZrBe-MG: 290 °C, Zr-MG: 403 °C and Ni-MG: 573 °C) and three BMGCs were investigated at different temperatures. Temperature strongly influences hardness, Young's modulus, and activation energy for all materials. A pronounced effect on the activation volume can be

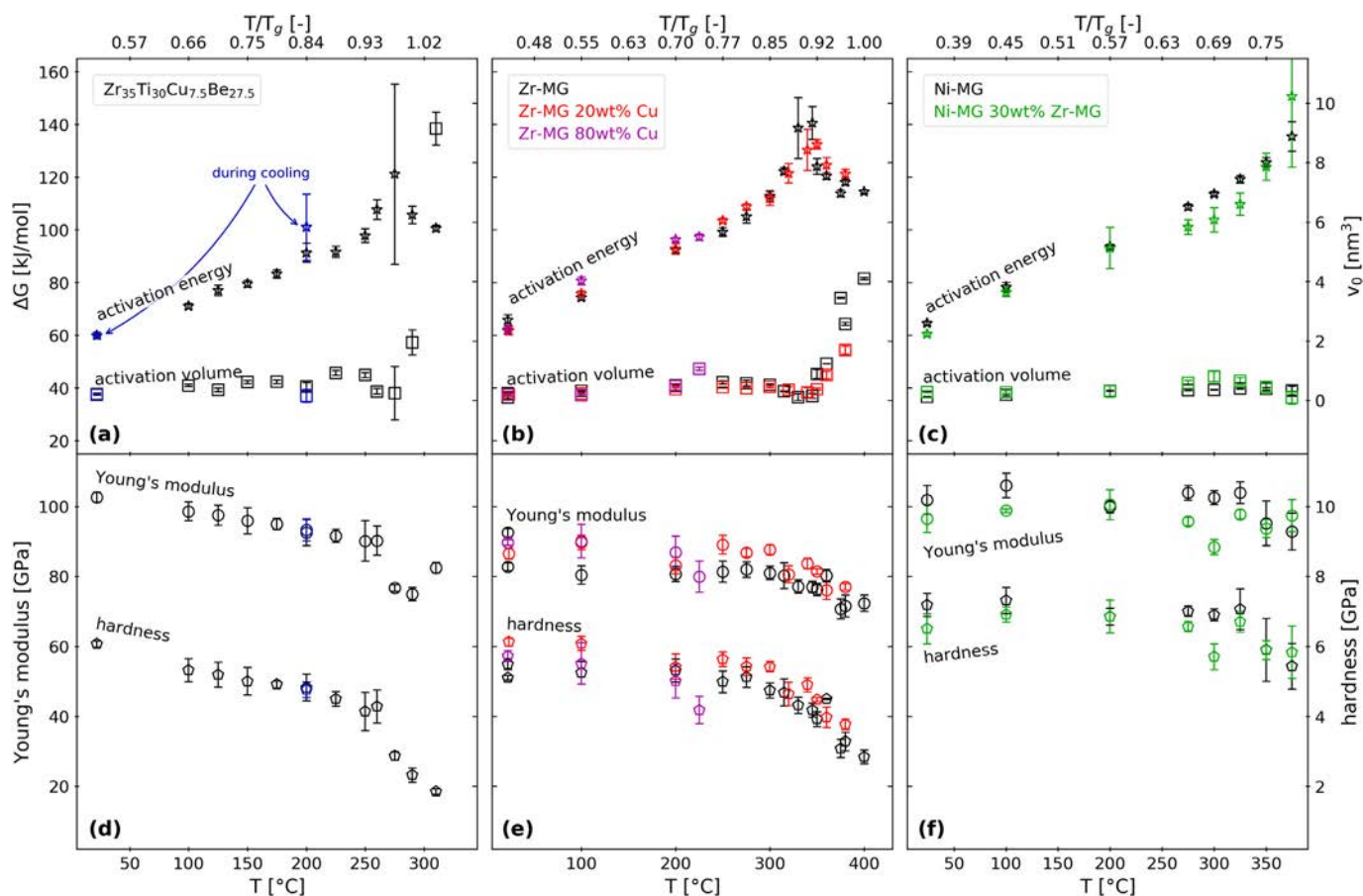


**Fig. 4.** Activation energy, volume, Young's modulus and hardness are plotted as function of temperature for three different BMGs and three different BMGCs. The respective homologous temperature is indicated on the top x-axis. Hardness and Young's modulus decrease with increasing temperature, more steeply at  $T$  approaching  $T_g$ . The activation stays nearly constant up to  $T_g$  and then shows a strong increase. The activation energy increases until  $T_g$  is reached and subsequently drops.

seen for materials, which have a lower  $T_g$  than the maximal testing temperature. This could not be observed for Ni-MG and Ni-MG 30 wt% Zr-MG, because the testing temperature does not exceed  $T_g$ . For all other materials a pronounced change of the properties correlating with a change in the slope of the curve for all measured and calculated properties can be observed at  $T_g$ . Hardness and Young's modulus decrease stronger at temperature higher  $T_g$ . The activation volume increases slowly when approaching  $T_g$ , but at higher temperatures  $v_0$  increases with a very high rate. In [34,56–59] similar values of several atomic volumes for the activation volumes at room temperature are shown. The activation energy shows also an increase for temperature below  $T_g$ , but decreases and levels off exceeding this temperature. The increase of activation energy was already shown in former studies by means of DSC measurements with different heating rates [60–62] and dilatometer experiments combined with synchrotron measurements [13]. Changes in the activation energy mean a change in the deformation behavior. Considering the flow units in metallic glasses as shear transformation zones (STZ), diffusion processes are likely to govern shear

related deformation. At low temperatures, the activation volumes are small and so few atoms are sufficient. It is probable that mainly smaller atoms will contribute, which have a higher diffusivity and therefore, the activation energy needed will be lower. Increasing the activation volume forces more atoms to participate and larger atoms with lower diffusivity will therefore increase the activation energy. Above the glass transition temperature, the diffusion mechanism changes from diffusion in a solid to diffusion in a viscous-liquid [63,64]. The consequence is an increase in activation volume and decrease in activation energy as seen in Fig. 4. Looking at the homologous temperature, all materials behave similarly. The absolute values differ, as varying composition leads to a change in diffusion constants, but the number of participating atoms governs the main behavior from a strict solid diffusion to liquid diffusion at temperatures higher than  $T_g$ . Two of the BMGCs (Zr-MG 20 wt% Cu and Ni-MG 30 wt% Zr-MG) show nearly identical values to the respective BMG. Since very fine microstructures were tested where the minor phases already is partly dissolved [10,11], the properties of the major phase dominate. A shift of  $T_g$  is probable, because the composition is changed, but it is maybe too small to effectively change the behavior at the investigated temperatures. Furthermore, the technique used mainly tests the initiation of the deformation. Influences from phase boundaries should be investigated by other techniques, such as compression tests. The specimen with the highest percentage of Cu (Zr-MG 80 wt% Cu) and a coarser microstructure does show lower transition temperatures, but heavy oxidation during high temperature testing prevents a clear conclusion. In summary, the fabrication method does not influence the deformation behavior of the BMGs. BMG fabricated via HPT and cast ones show nearly the same activation volumes and energies at room temperature.

**Table 1**

Young's modulus, hardness, activation volume and activation Energy of ZrBe-MG subjected to HPT. No distinctive changes due to the applied shear strain is visible and even the variation of the activation volumes remain very small, especially compared to the changes at higher temperature.

Applied shear strain	E [GPa]	H [GPa]	$V_0$ [nm <sup>3</sup> ]	$\Delta G$ [kJ/mol]
0	102.6 ± 1.4	6.07 ± 0.09	0.21 ± 0.03	60 ± 1
125	110.1 ± 1.5	6.15 ± 0.06	0.27 ± 0.02	58.6 ± 0.4
500	109.3 ± 1.5	6.19 ± 0.2	0.11 ± 0.02	62.6 ± 0.9

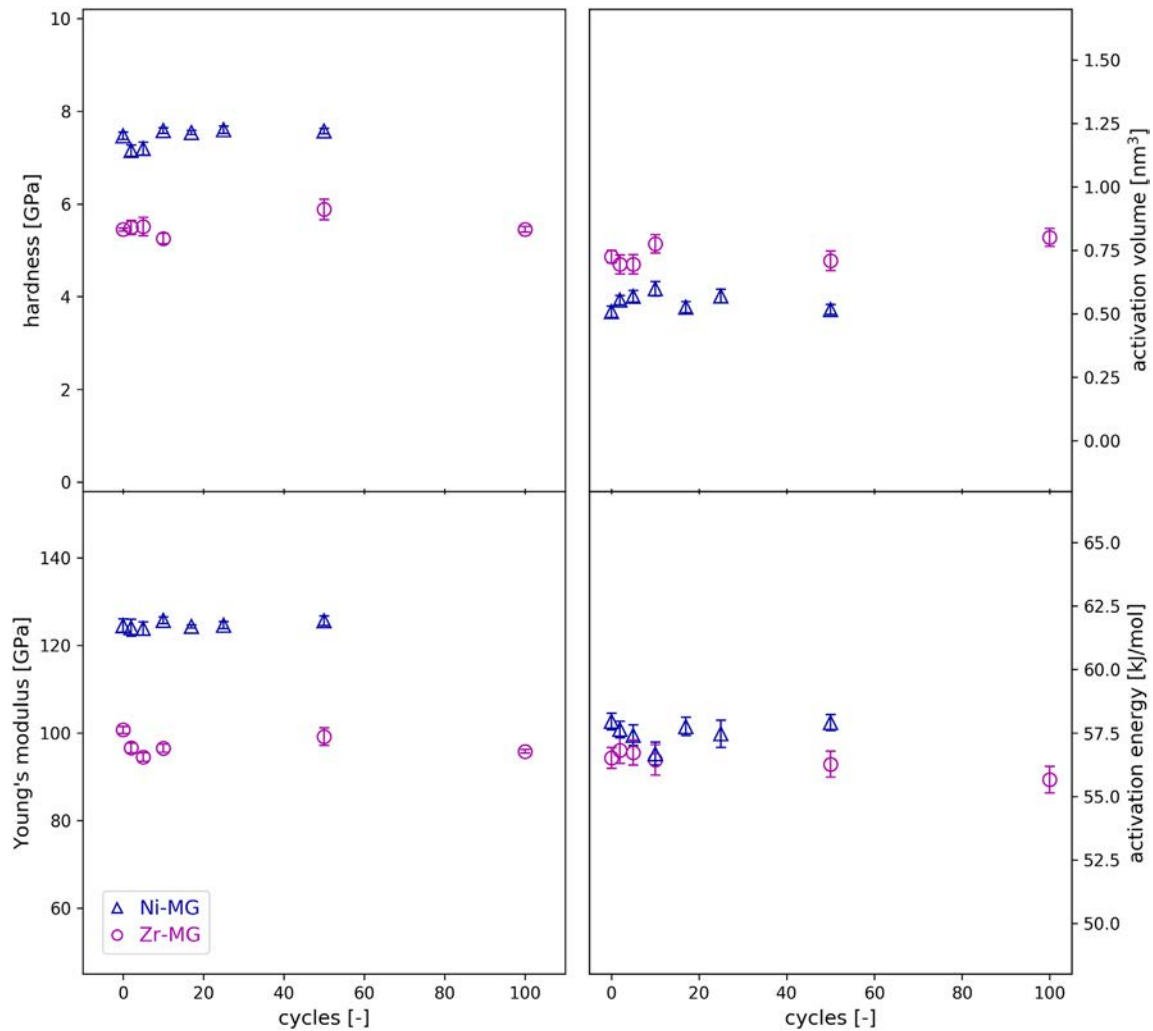


Fig. 5. Young's modulus, hardness, activation energy, and activation volume as functions of the number of thermal cycles. Zr-MG and Ni-MG sample were thermally cycled between room temperature and liquid nitrogen. No distinctive influences from the number of cycles is detectable.

To investigate rejuvenated MGs, HPT-deformation (Table 1) and thermal cycling (Fig. 5) was used, but no clear influence on activation energy and volume is detectable. In the literature, effects such as reduction in hardness and increase in the free volume are shown for some compositions. One explanation why nanoindentation does not show a difference for rejuvenated samples, is a heterogeneous distribution of free volume for instance. The small testing volume of nanoindentation (one indent probes only approximately  $1 \mu\text{m}^3$  to  $100 \mu\text{m}^3$ ) can make the detection difficult compared to methods which probe the whole specimens or larger volumes.

## 5. Conclusion

Three different BMGs (ZrBe-MG, Zr-MG and Ni-MG) and three composites (Zr-MG 20 wt% Cu, Zr-MG 80 wt% Cu and Ni-MG 30 wt% Zr-MG) were investigated by nanoindentation strain rate jump testing. In order to obtain different material states (as-casted, HPT-deformed, additional thermal cycling), the BMGs were subjected to high pressure torsion as well as thermal cycling. Additional nanoindentation tests were conducted at higher testing temperature up to  $430 \text{ }^\circ\text{C}$ . The main findings can be summarized by 5 points:

1) Nanoindentation strain rate jump tests can be used for estimating the activation volume and activation energy of BMGs.

- 2) The temperature has a great influence on the mechanical properties, especially when  $T_g$  is approached. All materials show a decrease in hardness and Young's modulus with increasing temperature and a drop in hardness when  $T_g$  is reached. The activation volume is stable at temperatures well below  $T_g$  and a strong increase is observed for temperatures near and higher than  $T_g$ . The activation energy increases up to  $T_g$ , but decreases again at higher temperatures. This is caused by a change in the diffusion mechanism. Below  $T_g$  solid diffusion with increasing number of participating atoms occurs and as  $T_g$  is exceeded, it changes to liquid diffusion.
- 3) The fabrication route does not significantly influence the activation volume and energy. The three BMGs behave similarly and onset temperatures of property changes accordingly to the respective  $T_g$ . Two of the composites (Zr-MG 20 wt% Cu and Ni-MG 30 wt% Zr-MG) behave like their main component, but Zr-MG 80 wt% Cu seems to show a derivation of its behavior with an earlier onset of softening and increasing of activation volume. Due to strong oxidation, it is not possible to draw a definite conclusion for this case.
- 4) High-pressure torsion causes no significant changes in hardness, Young's modulus and activation volume.
- 5) Thermal cycling weakly influences hardness and Young's modulus, but no significant change of the activation volume has been detected.

In conclusion, the activation volume and energy of different BMGs is mainly influenced by temperature and the selected composition, whereas thermal cycling or high-pressure torsion show no significant influence.

## Acknowledgments

We want to thank Alexander Leitner for the fruitful discussions and help in determining the constraint factors, and Jan Schroers and Liquidmetal® Technologies to supply us the ZrBe-BMG. The European Research Council under ERC Grant Agreement No. 3401 85 USMS has provided funding for this work. The financial support by the Austrian Federal Government (837900) within the framework of the COMET Funding Program (MPPE, A7.19) is highly appreciated.

## Data availability

Data will be made available on request.

## References

- [1] P. Murali, U. Ramamurty, Embrittlement of a bulk metallic glass due to sub-T<sub>g</sub> annealing, *Acta Mater.* 53 (2005) 1467–1478, <https://doi.org/10.1016/j.actamat.2004.11.040>.
- [2] Y.Q. Cheng, E. Ma, Intrinsic shear strength of metallic glass, *Acta Mater.* 59 (2011) 1800–1807, <https://doi.org/10.1016/j.actamat.2010.11.046>.
- [3] D.V. Louzguine-Luzgin, L.V. Louzguina-Luzgina, S.V. Ketov, V.Y. Zadorozhnyy, A.L. Greer, Influence of cyclic loading on the onset of failure in a Zr-based bulk metallic glass, *J. Mater. Sci.* (2014) 6716–6721, <https://doi.org/10.1007/s10853-014-8276-2>.
- [4] S.V. Ketov, Y.H. Sun, S. Nachum, Z. Lu, A. Checchi, A.R. Beraldin, H.Y. Bai, W.H. Wang, D.V. Louzguine-Luzgin, M.A. Carpenter, A.L. Greer, Rejuvenation of metallic glasses by non-affine thermal strain, *Nature* 524 (2015) 200–203, <https://doi.org/10.1038/nature14674>.
- [5] F. Meng, K. Tsuchiya, I. Seiichiro, Y. Yokoyama, Reversible transition of deformation mode by structural rejuvenation and relaxation in bulk metallic glass, *Appl. Phys. Lett.* 101 (2012) 121914, <https://doi.org/10.1063/1.4753998>.
- [6] X.D. Wang, Q.P. Cao, J.Z. Jiang, H. Franz, J. Schroers, R.Z. Valiev, Y. Ivanisenko, H. Gleiter, H. Ficht, Atomic-level structural modifications induced by severe plastic shear deformation in bulk metallic glasses, *Scr. Mater.* 64 (2011) 81–84, <https://doi.org/10.1016/j.scriptamat.2010.09.015>.
- [7] J. Pan, Y.X. Wang, Q. Guo, D. Zhang, A.L. Greer, Y. Li, Extreme rejuvenation and softening in a bulk metallic glass, *Nat. Commun.* 9 (2018) <https://doi.org/10.1038/s41467-018-02943-4>.
- [8] A. Hohenwarter, A. Bachmaier, B. Gludovatz, S. Scheriau, R. Pippan, Technical parameters affecting grain refinement by high pressure torsion, *Int. J. Mater. Res.* 100 (2009) 1653–1661, <https://doi.org/10.3139/146.110224>.
- [9] A. Vorhauer, R. Pippan, On the homogeneity of deformation by high pressure torsion, *Scr. Mater.* 51 (2004) 921–925, <https://doi.org/10.1016/j.scriptamat.2004.04.025>.
- [10] L. Krämer, Y. Champion, R. Pippan, From powders to bulk metallic glass composites, *Sci. Rep.* 7 (2017) 6651, <https://doi.org/10.1038/s41598-017-06424-4>.
- [11] L. Krämer, Y. Champion, K.S. Kormout, V. Maier-Kiener, R. Pippan, Bulk metallic dual phase glasses by severe plastic deformation, *Intermetallics* 94 (2018) <https://doi.org/10.1016/j.intermet.2017.12.005>.
- [12] L. Krämer, K. Kormout, D. Setman, Y. Champion, R. Pippan, Production of bulk metallic glasses by severe plastic deformation, *Metals* (Basel) 5 (2015) 720, <https://doi.org/10.3390/met5020720>.
- [13] A.R. Yavari, A. Le Moulec, A. Inoue, N. Nishiyama, N. Lupu, E. Matsubara, W.J. Botta, G. Vaughan, M. Di Michiel, Á. Kvikic, Excess free volume in metallic glasses measured by X-ray diffraction, *Acta Mater.* 53 (2005) 1611–1619, <https://doi.org/10.1016/j.actamat.2004.12.011>.
- [14] N. Matern, J. Bednarčík, S. Pauly, G. Wang, J. Das, J. Eckert, Structural evolution of Cu-Zr metallic glasses under tension, *Acta Mater.* 57 (2009) 4133–4139, <https://doi.org/10.1016/j.actamat.2009.05.011>.
- [15] K.M. Flores, D. Suh, R.H. Dauskardt, P. Asoka-Kumar, P.A. Sterne, R.H. Howell, Characterization of free volume in a bulk metallic glass using positron annihilation spectroscopy, *J. Mater. Res.* 17 (2002) 1153–1161, <https://doi.org/10.1557/JMR.2002.0171>.
- [16] Q.P. Cao, J.F. Li, Y.H. Zhou, A. Horsewell, J.Z. Jiang, Free-volume evolution and its temperature dependence during rolling of Cu<sub>60</sub>Zr<sub>40</sub> [20Ti] bulk metallic glass, *Appl. Phys. Lett.* 87 (2005) 101901, <https://doi.org/10.1063/1.2037858>.
- [17] V. Maier, K. Durst, J. Mueller, B. Backes, H.W. Höppel, M. Göken, Nanoindentation strain-rate jump tests for determining the local strain-rate sensitivity in nanocrystalline Ni and ultrafine-grained Al, *J. Mater. Res.* 26 (2011) 1421–1430, <https://doi.org/10.1557/jmr.2011.156>.
- [18] J.M. Wheeler, V. Maier, K. Durst, M. Göken, J. Michler, Activation parameters for deformation of ultrafine-grained aluminium as determined by indentation strain rate jumps at elevated temperature, *Mater. Sci. Eng. A* 585 (2013) 108–113, <https://doi.org/10.1016/j.msea.2013.07.033>.
- [19] W.J. Wright, R. Saha, W.D. Nix, Deformation mechanisms of the Zr<sub>40</sub>Ti<sub>14</sub>Ni<sub>10</sub>Cu<sub>12</sub>Be<sub>24</sub> bulk metallic glass, *Mater. Trans.* 42 (2001) 642–649, <https://doi.org/10.2320/matertrans.42.642>.
- [20] C.A. Schuh, T.G. Nieh, A Nanoindentation Study of Serrated Flow in Bulk Metallic Glasses, 51, 2003 87–99, <https://doi.org/10.1016/S>.
- [21] C.A. Schuh, A.C. Lund, T.G. Nieh, New regime of homogeneous flow in the deformation map of metallic glasses: elevated temperature nanoindentation experiments and mechanistic modeling, *Acta Mater.* 52 (2004) 5879–5891, <https://doi.org/10.1016/j.actamat.2004.09.005>.
- [22] L. Cheng, Z.M. Jiao, S.G. Ma, J.W. Qiao, Z.H. Wang, Serrated flow behaviors of a Zr-based bulk metallic glass by nanoindentation, *J. Appl. Phys.* 115 (2014) 0–5, <https://doi.org/10.1063/1.4866874>.
- [23] W. Liang, Z. Ning, Z. Dang, L. Wu, Plastic deformation behaviors of Ni- and Zr-based bulk metallic glasses subjected to nanoindentation, *Mater. Charact.* 86 (2013) 290–295, <https://doi.org/10.1016/j.matchar.2013.10.014>.
- [24] C.A. Schuh, T.C. Huftnagel, U. Ramamurty, Mechanical behavior of amorphous alloys, *Acta Mater.* 55 (2007) 4067–4109, <https://doi.org/10.1016/j.actamat.2007.01.052>.
- [25] T. Burgess, K.J. Laws, M. Ferry, Effect of loading rate on the serrated flow of a bulk metallic glass during nanoindentation, *Acta Mater.* 56 (2008) 4829–4835, <https://doi.org/10.1016/j.actamat.2008.05.039>.
- [26] F. Haag, D. Beitelshmidt, J. Eckert, K. Durst, Influences of residual stresses on the serrated flow in bulk metallic glass under elastostatic four-point bending – a nanoindentation and atomic force microscopy study, *Acta Mater.* 70 (2014) 188–197, <https://doi.org/10.1016/j.actamat.2014.01.053>.
- [27] H. Huang, J. Zhang, C.H. Shek, J. Yan, Effects of pre-compression deformation on nanoindentation response of Zr<sub>65</sub>Cu<sub>15</sub>Al<sub>10</sub>Ni<sub>10</sub> bulk metallic glass, *J. Alloys Compd.* 674 (2016) 223–228, <https://doi.org/10.1016/j.jallcom.2016.03.057>.
- [28] R. Limbach, K. Kosiba, S. Pauly, U. Kühn, L. Wondraczek, Serrated flow of CuZr-based bulk metallic glasses probed by nanoindentation: role of the activation barrier, size and distribution of shear transformation zones, *J. Non-Cryst. Solids* 459 (2017) 130–141, <https://doi.org/10.1016/j.jnoncrysol.2017.01.015>.
- [29] I.C. Choi, Y. Zhao, B.G. Yoo, Y.J. Kim, J.Y. Suh, U. Ramamurty, J. Il Jang, Estimation of the shear transformation zone size in a bulk metallic glass through statistical analysis of the first pop-in stresses during spherical nanoindentation, *Scr. Mater.* 66 (2012) 923–926, <https://doi.org/10.1016/j.scriptamat.2012.02.032>.
- [30] J.P. Coleman, F. Meng, K. Tsuchiya, J. Beadsworth, M. Leblanc, P.K. Liaw, J.T. Uhl, R.L. Weaver, K.A. Dahmen, Effect of annealing on nanoindentation slips in a bulk metallic glass, *Phys. Rev. B* 96 (2017) 1–9, <https://doi.org/10.1103/PhysRevB.96.134117>.
- [31] N. Thuriere, L. Perrière, M. Laurent-Brocq, Y. Champion, Activation volume in heterogeneous deformation of Mg<sub>65</sub>Cu<sub>12.5</sub>Ni<sub>12.5</sub>(Ce<sub>75</sub>La<sub>25</sub>)<sub>10</sub> metallic glass, *J. Appl. Phys.* 118 (2015) 0–5, <https://doi.org/10.1063/1.4936220>.
- [32] J.D. Ju, D. Jang, A. Nwankpa, M. Atzmon, An atomically quantized hierarchy of shear transformation zones in a metallic glass, *J. Appl. Phys.* 109 (2011) <https://doi.org/10.1063/1.3552300>.
- [33] M. Bletry, P. Guyot, Y. Brechet, J.J. Blandin, J.L. Soubeyrou, Homogeneous deformation of bulk metallic glasses in the super-cooled liquid state, *Mater. Sci. Eng. A* 387–389 (2004) 1005–1011, <https://doi.org/10.1016/j.msea.2004.02.085>.
- [34] F. Jiang, M.Q. Jiang, H.F. Wang, Y.L. Zhao, L. He, J. Sun, Shear transformation zone volume determining ductile-brittle transition of bulk metallic glasses, *Acta Mater.* 59 (2011) 2057–2068, <https://doi.org/10.1016/j.actamat.2010.12.006>.
- [35] G. Duan, A. Wiest, M.L. Lind, J. Li, W.K. Rhim, W.L. Johnson, Bulk metallic glass with benchmark thermoplastic processability, *Adv. Mater.* 19 (2007) 4272–4275, <https://doi.org/10.1002/adma.200700969>.
- [36] B. Sarac, J. Ketkaew, D.O. Popnoe, J. Schroers, Honeycomb structures of bulk metallic glasses, *Adv. Funct. Mater.* 22 (2012) 3161–3169, <https://doi.org/10.1002/adfm.201200539>.
- [37] B. Sarac, J. Schroers, Designing tensile ductility in metallic glasses, *Nat. Commun.* 4 (2013) 2158, <https://doi.org/10.1038/ncomms3158>.
- [38] L. Perrière, Y. Champion, Phases distribution dependent strength in metallic glass – aluminium composites prepared by spark plasma sintering, *Mater. Sci. Eng. A* 548 (2012) 112–117, <https://doi.org/10.1016/j.msea.2012.03.100>.
- [39] X.M. Wang, S.L. Zhu, H. Kimura, A. Inoue, Production of bulk glassy alloy parts by a levitation melting-forging method, *Mater. Trans.* 47 (2006) 2072–2075, <https://doi.org/10.2320/matertrans.47.2072>.
- [40] N.M. Everitt, M.I. Davies, J.F. Smith, High temperature nanoindentation – the importance of isothermal contact, *Philos. Mag.* 91 (2011) 1221–1244, <https://doi.org/10.1080/14786435.2010.496745>.
- [41] J.M. Wheeler, J. Michler, Invited article: indenter materials for high temperature nanoindentation, *Rev. Sci. Instrum.* 84 (2013) <https://doi.org/10.1063/1.4824710>.
- [42] B.N. Lucas, W.C. Oliver, Indentation power-law creep of high-purity indium, *Mettall. Mater. Trans. A* 30 (1999) 601–610, <https://doi.org/10.1007/s11661-999-0051-7>.
- [43] V. Maier, A. Hohenwarter, R. Pippan, D. Kiener, Thermally activated deformation processes in body-centered cubic Cr – how microstructure influences strain-rate sensitivity, *Scr. Mater.* 106 (2015) 42–45, <https://doi.org/10.1016/j.scriptamat.2015.05.001>.
- [44] G.M. Pharr, J.H. Strader, W.C. Oliver, Critical issues in making small-depth mechanical property measurements by nanoindentation with continuous stiffness measurement, *J. Mater. Res.* 24 (2009) 653–666, <https://doi.org/10.1557/jmr.2009.0096>.
- [45] W.C. Oliver, G.M. Pharr, Experiments, *J. Mater. Res.* 7 (1992) 1564–1583, <https://doi.org/10.1557/JMR.1992.1564>.
- [46] F. Spaepen, Defects in Amorphous Metals, 1982.
- [47] J.S. Langer, Shear-transformation-zone theory of plastic deformation near the glass transition, *Phys. Rev. E Stat. Nonlinear Soft Matter Phys.* 77 (2008) 1–14, <https://doi.org/10.1103/PhysRevE.77.021502>.
- [48] B. Yang, T.G. Nieh, Effect of the nanoindentation rate on the shear band formation in an Au-based bulk metallic glass, *Acta Mater.* 55 (2007) 295–300, <https://doi.org/10.1016/j.actamat.2006.08.028>.
- [49] D. Tabor, The hardness of solids, *Rev. Phys. Technol.* 1 (1970) 145–179, <https://doi.org/10.1088/0034-6683/1/3/101>.

- [50] A. Leitner, V. Maier-Kiener, D. Kiener, Essential refinements of spherical nanoindentation protocols for the reliable determination of mechanical flow curves, *Mater. Des.* 146 (2018) 69–80, <https://doi.org/10.1016/j.matdes.2018.03.003>.
- [51] W. Blum, Discussion: activation volumes of plastic deformation of crystals, *Scr. Mater.* 146 (2018) 27–30, <https://doi.org/10.1016/j.scriptamat.2017.10.029>.
- [52] M.Q. Jiang, M. Naderi, Y.J. Wang, M. Peterlechner, X.F. Liu, F. Zeng, F. Jiang, L.H. Dai, G. Wilde, Thermal expansion accompanying the glass-liquid transition and crystallization, *AIP Adv.* 5 (2015) <https://doi.org/10.1063/1.4939216>.
- [53] E. Pineda, I. Hidalgo, P. Bruna, T. Pradell, A. Labrador, D. Crespo, Structural study of conventional and bulk metallic glasses during annealing, *J. Alloys Compd.* 483 (2009) 578–581, <https://doi.org/10.1016/j.jallcom.2008.07.194>.
- [54] A.R. Yavari, S. Pang, D. Louzguine, A. Inoue, N. Lupu, N. Nikolov, G. Heunen, Change in thermal expansion coefficient of bulk metallic glasses T-g measured by real-time diffraction using high-energy synchrotron light, *J. Metastable Nanocryst. Mater.* 16 (2003) 105–110, <https://doi.org/10.4028/www.scientific.net/JMNM.15-16.105>.
- [55] A.P. Wang, T. Zhang, J.Q. Wang, Ni-based fully amorphous metallic coating with high corrosion resistance, *Philos. Mag. Lett.* 86 (2006) 5–11, <https://doi.org/10.1080/09500830500479718>.
- [56] Z.Q. Chen, L. Huang, P. Huang, K.W. Xu, F. Wang, T.J. Lu, Clarification on shear transformation zone size and its correlation with plasticity for Zr-based bulk metallic glass in different structural states, *Mater. Sci. Eng. A* 677 (2016) 349–355, <https://doi.org/10.1016/j.msea.2016.09.054>.
- [57] F. Spaepen, Homogeneous flow of metallic glasses: a free volume perspective, *Scr. Mater.* 54 (2006) 363–367, <https://doi.org/10.1016/j.scriptamat.2005.09.046>.
- [58] P. De Hey, J. Sietsma, A. Van Den Beukel, Structural disordering in amorphous Pd 40 Ni 40 P 20 induced by high temperature deformation, *Acta Mater.* 46 (1998) 5873–5882, [https://doi.org/10.1016/S1359-6454\(98\)00234-1](https://doi.org/10.1016/S1359-6454(98)00234-1).
- [59] P. Schall, D.A. Weitz, F. Spaepen, Structural rearrangements that govern flow in colloidal glasses, *Science* 318 (2007) 1895–1899, 80- <https://doi.org/10.1126/science.1149308>.
- [60] A. Cai, D. Ding, Y. Liu, H. Wu, W. An, G. Zhou, Y. Luo, Y. Peng, A series of Zr-based bulk metallic glasses with room temperature plasticity, *Materials (Basel)* 9 (2016) <https://doi.org/10.3390/ma9060408>.
- [61] S.X. Wang, S.G. Quan, C. Dong, Kinetic of glass transition of Zr<sub>57.2</sub>Al<sub>21.4</sub>Ni<sub>21.4</sub> bulk metallic glass, *Thermochim. Acta*, Elsevier B.V 2012, pp. 92–95, <https://doi.org/10.1016/j.tca.2010.12.005>.
- [62] K. Knorr, M.P. Macht, K. Freitag, H. Mehrer, Self-diffusion in the amorphous and supercooled liquid state of the bulk metallic glass Zr<sub>46.75</sub>Ti<sub>8.25</sub>Cu<sub>7.5</sub>Ni<sub>10</sub>Be<sub>27.5</sub>, *J. Non-Cryst. Solids* 250–252 ( (1999) 669–673, [https://doi.org/10.1016/S0022-3093\(99\)00157-X](https://doi.org/10.1016/S0022-3093(99)00157-X).
- [63] U. Geyer, S. Schneider, W.L. Johnson, Y. Qiu, T.A. Tombrello, M.P. Macht, Atomic diffusion in the supercooled liquid and glassy states of the Zr<sub>41.2</sub>Ti<sub>13.8</sub>Cu<sub>12.5</sub>Ni<sub>10</sub>Be<sub>22.5</sub> alloy, *Phys. Rev. Lett.* 75 (1995) 2364, <https://doi.org/10.1103/PhysRevLett.75.2364>.
- [64] X.P. Tang, U. Geyer, R. Busch, W.L. Johnson, Y. Wu, Diffusion mechanisms in metallic supercooled liquids and glasses, *Nature* 402 (1999) 160–162, <https://doi.org/10.1038/45996>.